JPE

Models and Experiments for the Main Topologies of MRC-WPT Systems

Mingbo Yang*, Peng Wang†, Yanzhi Guan* and Zhenfeng Yang*
*,†Department of Mechanical and Material Engineering, North China University of Technology, Beijing, China

Abstract

Models and experiments for magnetic resonance coupling wireless power transmission (MRC-WPT) topologies such as the chain topology and branch topology are studied in this paper. Coupling mode theory based energy resonance models are built for the two topologies. Complete energy resonance models including input items, loss coefficients, and coupling coefficients are built for the two topologies. The storage and the oscillation model of the resonant energy are built in the time domain. The effect of the excitation item, loss item, and coupling coefficients on MRC systems are provided in detail. By solving the energy oscillation time domain model, distance enhancing models are established for the chain topology, and energy relocating models are established for the branch topology. Under the assumption that there are no couplings between every other coil or between loads, the maximum transmission capacity conditions are found for the chain topology, and energy distribution models are established for the branch topology. A MRC-WPT experiment was carried out for the verification of the above model. The maximum transmission distance enhancement condition for the chain topology, and the energy allocation model for the branch topology were verified by experiments.

Key words: wireless power transfer, repeater, multi-loads, transmission efficiency

I. INTRODUCTION

Compared with traditional inductive coupling wireless power transfer technology and capacitive coupling wireless power transfer, Magnetic Resonance Coupling-Wireless Power Transfer (MRC-WPT) has the advantages of a greater transmission distance, lower requirements for alignment and so on. Therefore, this technology has received a lot of attention from researchers all over the world [1]-[4].

MRC-WPT has good topological characteristics [5][6]. The main topology of the MRC-WPT can take the form of the chain topology structure or the branch topology structure, as shown in fig.1. The chain topology has a prominent advantage in extending the distance of the wireless energy transmission, and the branch topology can be applied in multi-load applications. Therefore, these topologies are a significant research area for MRC-WPT to be widely applied. This work mainly focuses on finding the rules of the energy resonance for the chain and branch topologies. This can help to enlarge the applying scope of this new technology.

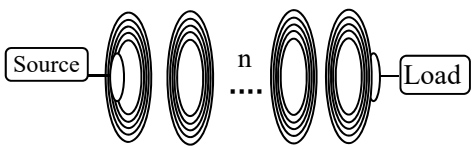

(A) Chain topology.

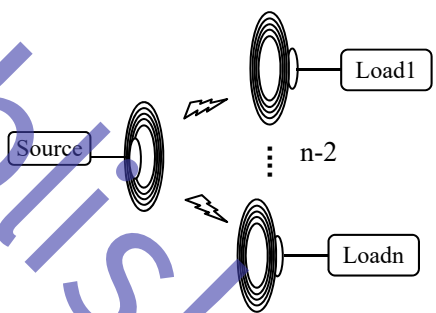

(B) Branch topology.

Fig.1 Structure diagram of chain topology and branch topology.

Recently, research on WPT has been mainly focused on improving transmission efficiency [7][8], driving circuit design [9], frequency tracking [10], placement design [11], impedance matching design [12], power detection [13], range detection, etc. In these areas, a great deal of progress has been made by researchers.

There has not been a lot of research on MRC-WPT topologies. Reference [14] introduced a case of the chain topology, referred to as the domino structure. A method has been proposed to optimize the transmission efficiency of the chain topology based on frequency adjustment and load optimization. The efficiency of the chain topology was studied by using the equivalent circuit method. A new optimization scheme for the multi load topology was proposed in [15] and [16]. Based on the method of process optimization, the transmission capacity and transmission

efficiency of the system can be improved under the multi-load topology. In addition, by using the Lagrange duality theory, the convergence interval of the optimal control is found. In [17], energy transfer control of loads with different frequency characteristics is realized through the frequency control method (band pass and band stop). Although this method has been used to change the system impedance, other factors that affect the system impedance such as the coupling coefficient, load variation and excitation change were not taken into account. In addition, the energy distribution law between multiple loads was rarely mentioned. Reference [18] proposed an integrator PLL based direct phase control (DPC) approach to provide accurate frequency-tracking for WPT systems. This method can help frequency tracking. However, the injection of current changes the resonance point of the circuit and lowers the Q value of the sending system. Therefore, it needs to be improved for wide application of MRC-WPT systems.

Based on previous research findings, two basic forms of the MRC topology, namely the chain topology and the branch topology, are studied and discussed. Energy propagation, transmission characteristics analysis and experimental verification have been thoroughly studied for the two topologies. The main topology characteristics of MRC wireless power transmission were provided in this paper.

II. ENERGY DISTRIBUTION MODEL OF THE TOPOLOGICAL STRUCTURE

A. *Chain topology structure*

The chain topology utilizes one or more resonance coils between the sending coil and the receiving coil to enhance the magnetic resonance coupling phenomenon. Then, the range of the whole wireless power transmission can be effectively extended.

(1) The chain topology structure model of *n-2* resonant repeaters:

$$\begin{pmatrix} \frac{d\vec{a}_1}{dt} \\ \frac{d\vec{a}_2}{dt} \\ \vdots \\ \frac{d\vec{a}_n}{dt} \end{pmatrix} = \begin{pmatrix} (\text{-j})(\omega_s - j\Gamma_S) & jk_{12} & & jk_{1n} \\ jk_{21} & (\text{-j})(\omega_s - j\Gamma_S) & & jk_{2n} \\ & & \ddots & \\ jk_{n1} & jk_{n2} & & (\text{-j})(\omega_s - j\Gamma_S) \end{pmatrix} \begin{pmatrix} \vec{a}_1 \\ \vec{a}_2 \\ \vdots \\ \vec{a}_n \end{pmatrix} \quad (1)$$

Where, n represents the total number of resonant bodies, $\vec{a}_n$ represents the mode value of the energy stored in the *n*th resonance coil, ω_s represents the operating frequency of the MRC system, k_{ij} represents the coupling coefficient between the *i* resonator and the *j* resonator, and Γ_S represents the loss coefficient of the resonator. Suppose that the loss coefficient of each coil is the same.

The given initial condition as formula (2).

$$\begin{cases} k_1 = k_{12} = k_{21} \\ k_2 = k_{23} = k_{32} \\ \vec{x}(0) = \left(\vec{a}_1(0), \vec{a}_2(0), \vec{a}_3(0)\right) = \left(A_{ini}, 0, 0\right) \end{cases} \quad (2)$$

The solution of formula (1) is shown by formula (3).

$$\begin{pmatrix} |a_1(t)|^2 \\ |a_2(t)|^2 \\ |a_3(t)|^2 \end{pmatrix} = \begin{pmatrix} \frac{A_{ini}^2}{4\left(k_2^2 + k_1^2\right)^2} e^{-2\Gamma_S t}\left(k_1^2 2\cos(t\sqrt{k_2^2 + k_1^2}) + 2k_2^2\right)^2 \\ \frac{A_{ini}^2 k_1^2}{4\left(k_2^2 + k_1^2\right)^2} e^{-2\Gamma_S t}\left(2\sin(t\sqrt{k_2^2 + k_1^2})\right)^2 \\ \frac{A_{ini}^2 k_1^2 k_2^2}{4\left(k_2^2 + k_1^2\right)^2} e^{-2\Gamma_S t}\left(2\cos(t\sqrt{k_2^2 + k_1^2}) - 2\right)^2 \end{pmatrix} \quad (3)$$

The energy model of the three resonant coils includes three parts, which are the module value term, the loss term and the phase term. The energy phase difference between $a_1(t)$, $a_2(t)$ and $a_3(t)$ is $\frac{\pi}{2}$. From the expression of the $|a_3(t)|^2$ item, it can be concluded that the energy received by the receiving coil will reach the maximum point when the coupling coefficient k12 is equal to k23 under the condition of k12+k23$\leqslant M$. The value of *M* is constant because the total distance between the sending coil and the receiving coil is definitive. Therefore, the value of k_{12}+k_{23} has an upper limit, and *M* is given as 0.9 for numerical modeling.

(2) The zero input response with excitation and loss items.

When the input item *F* and loss coefficient Γ_s are set to zero, the energy propagation model can be calculated as Figure 1(a). The curves with circles, triangles and squares correspond to the energy resonance of the sending coil, the relay coil and the receiving coil, respectively. The X axis is the time axis and the Y axis is the energy axis. Since the three coils have the same resonance frequency, and the operating frequency is equal to the resonance frequency, the energy resonance path is established. At the beginning, the energy stored in the sending coil is in the state of LC resonance. Then the energy is emitted by way of the magnetic coupling link with the repeater and received by it. Next, the energy reaches the receiving resonant coil through the magnetic link between the repeater and the receiver. Because of the absence of a load, the energy goes back to the sending coil and moves back and forth as the flowing routine:

Source(S)→Repeater(R)→Receiver(D)→Repeater(R)→Source(S)→Repeater(R)→……

The details are shown in fig.2. Unlike induction coupling applications, the energy exchanging of the resonance coupling system does not follow the sinusoidal rule. The energy peaks of both the sending coil and the receiving coil last for a short time while the low energy state last longer.

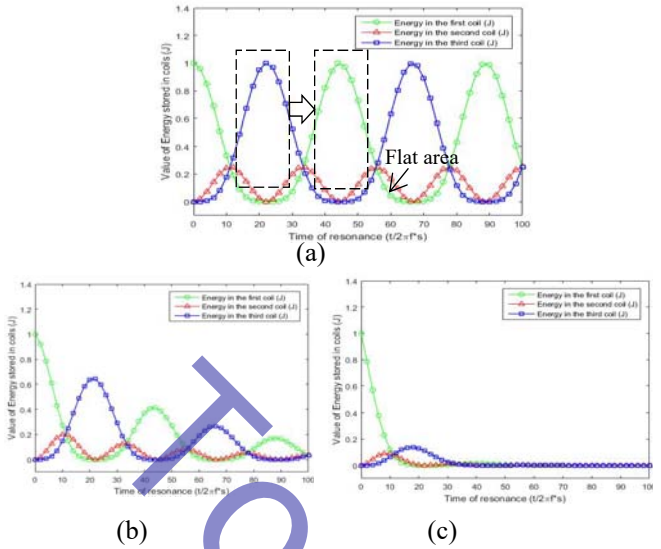

(a) (b) (c)

Fig.2 Energy distribution model of the single repeater MRC-WPT.

With a nonzero loss item, which includes but is not limited to resistive loss and radiation loss, the energy of the resonance system gradually dissipates. Figure 2 (b) shows the situation under which $\Gamma_s = 0.01$ and Figure 2 (c) shows the case of $\Gamma_s = 0.05$. When the loss coefficient is introduced to the system, the energy oscillation is weaken and the stored energy is consumed by the resistive loss and radiation loss. The bigger the loss coefficient is, the less the magnetic energy will last. Therefore, choosing a high Q-value resonance coil is very important for building an efficient MRC setup. A coil with a low Q-value cannot meet the resonance requirements for near field energy resonance.

The above analysis gives an analysis of the energy oscillations in ideal situations with $k_1 = k_2$. As for the general situation, different situations of the coupling coefficients are introduced into the model.

a. k_1=0.1, k_2=0.3 and k_1=0.3, k_2=0.1.

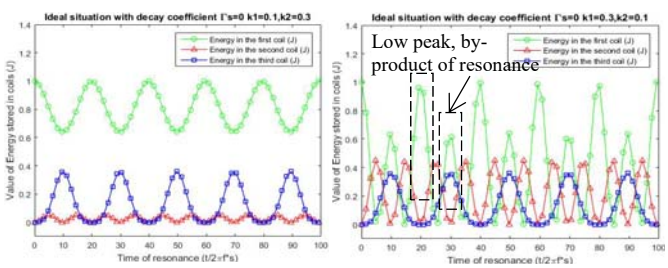

(a) k_1=0.1，k_2=0.3. (b) k_1=0.3，k_2=0.1.

Fig.3 Oscillatory energy distribution under different coupling coefficients.

Under the situation of k_1=0.1, k_2=0.3, resonance coil is set closer to the sending coil than the receiving coil, and energy distribution is shown in figure 3(a).

Because of a smaller k_1, the coupling between the sending coil and the repeater is weak. Most of the energy is constrained by the S coil, and little energy is transmitted to the receiving coil by way of the repeater. In this situation, the energy stored in the receiving coil never exceeds 40% of the total energy stored in source coil. On the other hand, the energy stored in the source coil stays higher than 60% of the total initial energy. The repeater coil can hold small amount of energy and it can maintain this energy by doubling the resonance frequency when compared to the working frequency. Therefore, in the case of $k_1<k_2$, most of the energy is held by the sending coil, and the power transmission efficiency is low when compared to the $k_1=k_2$ situation.

The situation of k_1=0.3, k_2=0.1 is shown in figure 3(b). The coupling between the source coil and the repeater coil is stronger than it is between the repeater coil and the receiving coil. Since another resonance body exists in the source coil's near field (k_1 is 0.3), the sending coil can perform full energy exchanging (the energy fluctuates between the empty state 0 and the full state 1) with its resonance energy outlet, which is made up of the repeater coil and the receiving coil. In this situation, the energy exchanging frequency between the source coil and the repeater coil is doubled when compared to case (a), and frequency splitting phenomenon appeared due to the strong coupling between the sending coil and the repeater coil. Main energy oscillations occur between the source coil and the repeater coil, whereas the receiving coil keeps exchanging energy with the union of the sending coil and repeater coil in the undoubled working frequency. Furthermore, as for odd energy oscillation, the receiving coil is synchronous with the repeater coil by absorbing energy from the source coil. As for the even energy oscillation process, the receiving coil is synchronous with the source coil in terms of absorbing energy from the repeater coil. Briefly, most of the energy of the system is concentrated on the two resonance coils and the receiving coil can derive a little energy from the strong coupling union of the sending coil and the receiving coil. Therefore, the power transmission efficiency is still lower than the situation $k_1=k_2$.

b. k_1=0.2,k_2=0.03 and k_1=0.03,k_2=0.2.

For further analysis of the $k_1 \neq k_2$ situation, experimental results of the extreme situation are given in figure 4.

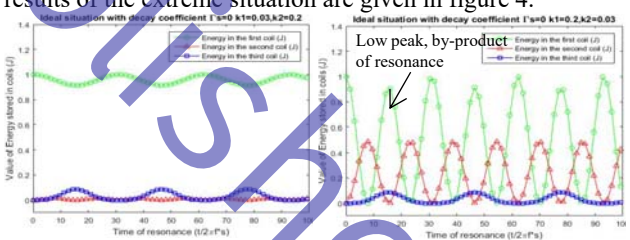

(a) k_1=0.03，k_2=0.2. (b) k_1=0.2，k_2=0.03.

Fig.4 Energy distribution with different coupling coefficients.

The extreme coupling coefficient condition is given, as shown in figure 4. The overall coupling relationship among the three resonance coils is the same as that of the experiment introduced above. However, there are still important differences. From figure 4 (a), under the situation k_1=0.03, k_2=0.2, the energy exchanging period is prolonged when compared to the situation as shown in figure 3. A weaker coupling coefficient k_1 slows the energy exchanging frequency between the S coil and the R coil, and between the R coil and the D coil. Because k_1 is set smaller, the energy is chocked in the S coil and can barely be received by the repeater coil. On the other hand, as shown in figure 4 (b), when k_1=0.2, k_2=0.03, since k_2=0.03 is small when compared to k_1=0.2, the D coil has a slight influence on the resonance between the S coil and the R coil, and a little energy is

transmitted to the D coil. At this time, the S coil and the R coil compose one strong resonance coupling pair which holds most of the power in the system. Since a weak coupling still exists, the D coil still periodically exchanges energy with the R coil, and the exchanging frequency is lowered because of the existence of the D coil.

For the $\Gamma_s \neq 0$ situation, when k_1=0.2, k_2=0.03, the magnetic energy decay phenomenon is as shown in figure 5. Under this situation, the magnetic energy is losing very fast, and the higher the loss coefficient is, the sooner magnetic energy exhausts to zero. In addition, the receiving coil can get very little energy in this situation. Therefore, it is difficult for the MRC system to output power with the parameters given above.

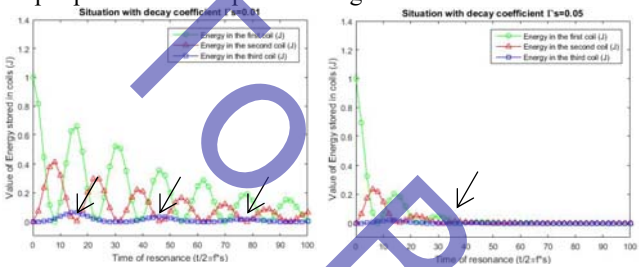

(A) $\Gamma_s = 0.01$. (B) $\Gamma_s = 0.05$.

Fig. 5 Energy distribution with different loss coefficients where k_1=0.02, k_2=0.2.

From the analysis above, it can be concluded that:

a. Case 1: $\Gamma_s = 0$, when $k_1<k_2$, the energy oscillation amplitude is weaker than that in the condition $k_1=k_2$. The energy was mainly stored in the source coils in form of LC oscillation. When $k_1>k_2$, the energy oscillation is still weaker than that in the situation of $k_1=k_2$. In this situation, most of the energy oscillates between the sending coil and the repeater coil. In both situations, the receiving coil can get less energy from the S coil and the R coil when compared to the $k_1=k_2$ situation. The value of the coupling coefficient is exchanged from the two situation as:

$$\begin{cases} k_1 = k_2' \\ k_2 = k_1' \end{cases} \tag{4}$$

The working principle of the repeater is kept the same and the energy exchanging frequency is kept unchanged as well.

b. Case 2: $\Gamma_s \neq 0$. In this situation, the initial energy was quickly lost through the resistance loss and the radiation loss. The energy transmission regularity complies with case 1.

c. Case3: the energy exchange frequency is influenced by the coupling coefficient between the resonance coils. As for a higher coupling coefficient, the power exchanging frequency between the two resonance coils is higher than that system with a lower coupling coefficient. However, the efficiency of the system is constrained at the same time. A higher working frequency leads to a heavier energy loss. Therefore, using high value Q coil is a good choice to improve the transmission capacity and efficiency at the same time. The energy exchanging frequency f_{pex} is a nonlinear function of the coefficients:

$$\begin{cases} f_{pex} = \Theta(k_1, k_2, ..., k_n) \\ f_{pex} \propto k_1, k_2, ..., k_n \end{cases} \tag{5}$$

d. When $k_1=k_2$, the receiving coil can get a maximum amount of energy, and the resonance system can output energy at the maximum capacity and maximum efficiency.

$$P_{max} = P_{k_1=k_2} \tag{6}$$

(3) Zero state response with excitation and loss items.

The driving signal is taken into account for studying the excitation response of the repeater system in this section.

a. $\Gamma_s = 0$

Firstly, in ideal working conditions, when the loss coefficient is set zero, energy distribution is calculated as formula (7).

$$\begin{pmatrix} |a_1(t)|^2 \\ |a_2(t)|^2 \\ |a_3(t)|^2 \end{pmatrix} = \begin{pmatrix} \frac{1}{4\left(k_2^2+k_1^2\right)^3}\left(2k_1^2\sin(t\sqrt{k_2^2+k_1^2})+2k_2^2tF\sqrt{k_2^2+k_1^2}\right)^2 \\ \frac{k_1^2F^2}{\left(k_2^2+k_1^2\right)^2}\left(\cos(t\sqrt{k_2^2+k_1^2})-1\right)^2 \\ \frac{k_1^2k_2^2F^2}{4\left(k_2^2+k_1^2\right)^3}\left(\begin{pmatrix}\sin(2t\sqrt{k_2^2+k_1^2})-2t\sqrt{k_2^2+k_1^2} \\ \cos(t\sqrt{k_2^2+k_1^2})\end{pmatrix}^2 + \begin{pmatrix}\cos(t\sqrt{k_2^2+k_1^2})-1 \\ +2t\sqrt{k_2^2+k_1^2}\sin(t\sqrt{k_2^2+k_1^2})\end{pmatrix}^2\right) \end{pmatrix} \tag{7}$$

The distribution of the magnetic energy is shown in figure 6.

The input energy of the system comes from the *F(t)* item. Due to the absence of the loss and load, there is no energy consuming in the system. Therefore, the energy stored in the sending coil and the receiving coil keeps increases. During the energy accumulating process, energy exchanges between the resonance coils. The higher the coupling coefficient is, the higher the energy exchanging frequency becomes. As for the higher coupling coefficient instance, the energy density is very high when compared to the lower cases. A higher energy exchanging frequency makes the repeater coil's maximum amplitude of the energy lower when compared to the lower coupling coefficient cases. As for the lower coupling coefficient instance, the energy density is not very high when compared to the higher cases because the energy fluctuates substantially in form of oscillation. A lower energy exchanging frequency makes the repeater coil's maximum amplitude of the energy higher than the left case.

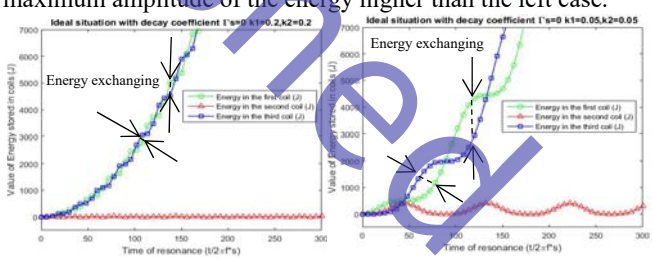

(A) $k_1=k_2=0.2$. (B) $k_1=k_2=0.05$.

Fig.6 Energy distribution of the MRC with an exciting function F(t).

When $k_1 \neq k_2$, the energy distribution is shown in figure 7; when $k_1 > k_2$, most of the energy is stored in the receiving coil; and when $k_1 < k_2$, more energy is stored in the sending coil. This is consistent with the conclusion of the former section. Furthermore, as is the case with no loss and load in the system, the total energy in the system is equal if the values of k_1 and k_2

are exchanged.

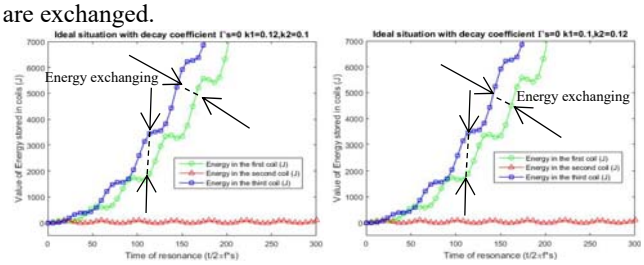

(A) k_1=0. 12 k_2=0. 1. (B) k_1=0. 1 k_2=0. 12.

Fig.7 Energy distribution of the MRC with an exciting function F(t).

b. $\Gamma_s \neq 0$

When the input item $F_{input}(t)$ is introduced and the loss coefficient is $\Gamma_s \neq 0$, the energy model can be deduced as formula (8).

$$\begin{pmatrix} |\vec{a}_1(t)|^2 \\ |\vec{a}_2(t)|^2 \\ |\vec{a}_3(t)|^2 \end{pmatrix} = \begin{pmatrix} \frac{F^2(e^{-t\Gamma_s}(2\Gamma_s^2\cos(tk\sqrt{2})-2\Gamma_s k\sqrt{2}\sin(tk\sqrt{2})+2\Gamma_s^2+4k^2)-4(\Gamma_s^2+k^2))^2}{16(\Gamma_s^2+2k^2)^2\Gamma_s^2} \\ F^2(\frac{\sqrt{2}e^{-t\Gamma_s}(2\Gamma_s\sin(tk\sqrt{2})+2k\sqrt{2}\cos(tk\sqrt{2}))}{4\Gamma_s^2+8k^2}-\frac{k}{\Gamma_s^2+2k^2})^2 \\ \frac{F^2e^{-2t\Gamma_s}(\Gamma_s^2\cos(tk\sqrt{2})-\Gamma_s k\sqrt{2}\sin(tk\sqrt{2})+2e^{t\Gamma_s}k^2-\Gamma_s^2-2k^2)^2}{4(\Gamma_s^2+2k^2)^2\Gamma_s^2} \end{pmatrix} \tag{8}$$

To reduce the computational load, the following is given: $k_1 = k_2 = k$. With the increase of the loss coefficient, the energy distribution of the relay coil and the resonant coils is shown in Figure 8. The circle, triangle and square curves represent the energy distribution of the sending coil (S), the repeater coil (R) and the receiving coil (D) in the time domain.

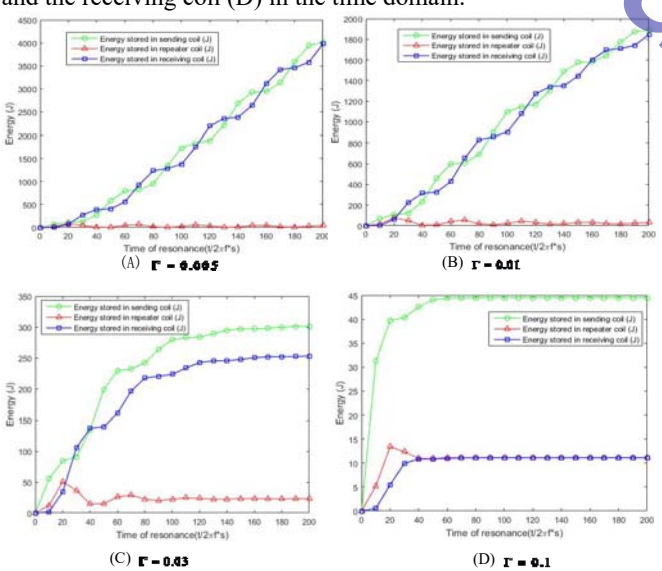

(A) Γ = 0.005 (B) Γ = 0.01

(C) Γ = 0.03 (D) Γ = 0.1

Fig.8 Energy distribution and consuming model of a single repeater with energy input and non-zero loss coefficient items.

As shown in figure 8, the input item provides energy for the system whereas the loss item consumes energy. With an increase of the loss coefficient, the energy stored in the system varies from consecutive increases to remain stable. In addition, the higher the loss coefficient is the lower the energy convergence value stays on. Therefore, in the ideal working state (low loss coefficient and strong coupling link), most of the energy stays in the S coil and D coil, and there is little energy stored in the repeater coil. When impedance matching is achieved, the energy passes the three coil channel with little loss. The repeater coil brings the loss item into the system. However, the increment of the loss is acceptable when compared to the increase in distance.

(4) Coupling coefficient variation.

When the coupling coefficient changes from high to low under the condition of a weak coupling between the resonance coils, it becomes difficult for the sending coil to emit energy, and the energy left in the resonant coil is gradually increased. At the same time, the energy absorbed by the receiving resonant coil decreases with the decrease of the coupling coefficient. When the coupling coefficient is high enough, energy can oscillate between the transmitting coil and the receiving coil. On the other hand, the oscillations disappear.

B. Branch topology structure

The branch topology includes mainly two types. The two types are the one-to-many structure and the many-to-one structure. The former topology provides energy to multiple loads. It also involves energy directional propagation and energy contention between the receivers. The latter topology includes multiple emission sources and one receiver. It can be applied in high current or high power charging cases. Unlike the one-to-many topology, circuit protection issues should be concerned in the many-to-one topology to avoid the damage caused by energy flowing mutually between the sources.

(1) Branch topology model of n-1 output.

$$\begin{pmatrix} \frac{d\vec{a}_1}{dt} \\ \frac{d\vec{a}_2}{dt} \\ \vdots \\ \frac{d\vec{a}_n}{dt} \end{pmatrix} = \begin{pmatrix} (\text{-j})(\omega_s - j\Gamma_S) & jk_{12} & & jk_{1n} \\ jk_{21} & (\text{-j})(\omega_s - j\Gamma_S) & & jk_{2n} \\ & & \ddots & \\ jk_{n1} & jk_{n2} & & (\text{-j})(\omega_s - j\Gamma_S) \end{pmatrix} \begin{pmatrix} \vec{a}_1 \\ \vec{a}_2 \\ \vdots \\ \vec{a}_n \end{pmatrix} + \begin{pmatrix} Fe^{-j\omega t} \\ 0 \\ \vdots \\ 0 \end{pmatrix} \tag{9}$$

Where, n represents the total number of resonant bodies, $\vec{a}_n$ represents the mode value for the energy of the resonance coils, ω_s represents the operating frequency of the system, k_{ij} represents the coupling coefficient between the first i resonator and the j resonator, and Γ_s represents the loss coefficient of the resonator. Here, the loss coefficients of each coil are assumed to be equal. The $Fe^{-j\omega t}$ item represents the external input.

a) Unlike the chain topology, the coupling between loads cannot be ignored here, and the coupling for all of the resonant bodies should be included in the model.

b) As for two load applications, the CMT function can be expressed as formula (10).

$$\begin{pmatrix} \frac{d\vec{a}_1}{dt} \\ \frac{d\vec{a}_2}{dt} \\ \frac{d\vec{a}_3}{dt} \end{pmatrix} = \begin{pmatrix} \text{-j}\,\omega_s - \Gamma_S & \text{j}\,k_{12} & jk_{13} \\ \text{j}\,k_{12} & \text{-j}\,\omega_s - \Gamma_S & \text{j}\,k_{23} \\ jk_{31} & \text{j}\,k_{23} & \text{-j}\,\omega_s - \Gamma_S \end{pmatrix} * \begin{pmatrix} \vec{a}_1 \\ \vec{a}_2 \\ \vec{a}_3 \end{pmatrix} + \begin{pmatrix} Fe^{-j\omega t} \\ 0 \\ 0 \end{pmatrix} \tag{10}$$

Where, k_{12} is the coupling coefficient between the sending coil and load1, k_{13} is the coupling coefficient between the sending coil and load2, and k_{23} is the coupling coefficient between the two loads.

(2) Energy distribution analysis.

a) Zero input response.

Initial condition:

$$\begin{cases} \Gamma_s = 0 \\ \{a_1(0), a_2(0), a_3(0)\} = \{1, 0, 0\} \\ F = 0 \end{cases} \tag{11}$$

The analytical solution of the energy distribution model can be deduced as formula (12).

$$\begin{pmatrix} |a_1(t)|^2 \\ |a_2(t)|^2 \\ |a_3(t)|^2 \end{pmatrix} = \begin{pmatrix} e^{(-2\Gamma_s t)} \cos(t\sqrt{k_{12}^2 + k_{13}^2})^2 \\ \frac{1}{k_{12}^2 + k_{13}^2} k_{12}^2 e^{(-2\Gamma_s t)} \sin(t\sqrt{k_{12}^2 + k_{13}^2})^2 \\ \frac{1}{k_{12}^2 + k_{13}^2} k_{13}^2 e^{(-2\Gamma_s t)} \sin(t\sqrt{k_{12}^2 + k_{13}^2})^2 \end{pmatrix} \tag{12}$$

The energy distribution is shown in figure 9.

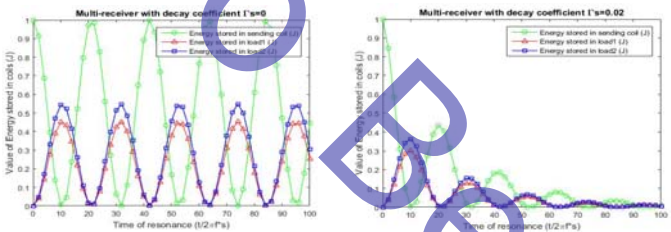

(A) $\Gamma=0, F=0$ (B) $\Gamma=0.02, F=0$

Fig.9 Energy distribution model of the two loads application without an input excitation.

The circle curve represents the energy distribution of the sending coil. The triangle curve and the square curve represent the energy distributions of load1 and load2, respectively. When the coupling coefficient k_{13} is higher than k_{12}, coil 2 stores more energy than coil 1. Then, load 2 receives more energy than load 1 and the phase of energy between each load is consistent. It can be seen that the ratio of the received energy is proportional to the square of the coupling coefficient k_{12}, k_{13} from formula (12). Namely:

$$W_1 : W_2 = {k_{12}}^2 : {k_{13}}^2 \tag{13}$$

b) Zero state response.

Initial condition:

$$\begin{cases} \Gamma_s = 0.05 \\ \{a_1(0), a_2(0), a_3(0)\} = \{0, 0, 0\} \\ F = 1 \end{cases} \tag{14}$$

Then, by solving the mode function, the energy distribution result is as formula (15).

$$\begin{pmatrix} |a_1(t)|^2 \\ |a_2(t)|^2 \\ |a_3(t)|^2 \\ M \end{pmatrix} = \begin{pmatrix} \frac{F^2(-e^{-t\Gamma_s}\cos(t\sqrt{k_{12}^2+k_{13}^2})\Gamma_s + e^{-t\Gamma_s}\sin(t\sqrt{k_{12}^2+k_{13}^2})\sqrt{k_{12}^2+k_{13}^2}+\Gamma_s)^2}{(k_{12}^2+k_{13}^2+{\Gamma_s}^2)^2} \\ \frac{{k_{12}}^2 F e^{-2t\Gamma_s} M}{(k_{12}^2+k_{13}^2+{\Gamma_s}^2)^2(k_{12}^2+k_{13}^2)} \\ \frac{{k_{13}}^2 F e^{-2t\Gamma_s} M}{(k_{12}^2+k_{13}^2+{\Gamma_s}^2)^2(k_{12}^2+k_{13}^2)} \\ \begin{pmatrix} (k_{12}^2+k_{13}^2-{\Gamma_s}^2)\cos(t\sqrt{k_{12}^2+k_{13}^2})^2 - 2e^{t\Gamma_s}\sqrt{k_{12}^2+k_{13}^2}\sin(t\sqrt{k_{12}^2+k_{13}^2})\Gamma_s \\ +(2\sqrt{k_{12}^2+k_{13}^2}\sin(t\sqrt{k_{12}^2+k_{13}^2})\Gamma_s - 2e^{t\Gamma_s}(k_{12}^2+k_{13}^2))\cos(t\sqrt{k_{12}^2+k_{13}^2}) \\ +(k_{12}^2+k_{13}^2)e^{2t\Gamma_s}+{\Gamma_s}^2 \end{pmatrix} \end{pmatrix} \tag{15}$$

The energy distribution of the system is shown in Fig10.

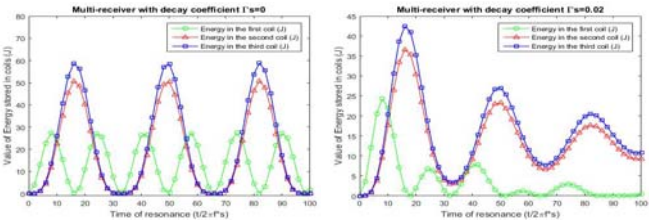

(A) $\Gamma=0, F=e^{-\Gamma_s t}$ (B) $\Gamma=0.02, F=e^{-\Gamma_s t}$

Fig.10 Energy distribution model of the two loads application with an input excitation.

As is shown in Figure 10 (A), if the loss coefficient is set to zero, the energy exchange period of the coils is half the period of the sending coil. However, the amplitude is higher than the amplitude of the sending coil. Therefore, in the process of the multi load energy transfer, the amplitude of the oscillation energy of the sending coil is decreased by the loads. However, the oscillation frequency is doubled when compared to the loads in the two loads case. Figure 10 (B) shows the result of the numerical simulation when the coefficient is set to 0.02. The system's ability to store energy fades down, and the energy exchange capacity between the coils is reduced by the loss item.

In figure (B), the oscillation of energy vanishes if the x axis is long enough. This does not comply with the law of the multi-load instance since the general energy distribution should be periodic (not constant). This is mainly caused by the incomplete model that was set up. In this model, the loss coefficient is assigned to be scalar data. Meanwhile, in a real MRC system, the loss coefficient should be complex because the varying of the phase of the current results in varying of the resistive losses and radiation loss during LC oscillations. However, in the coupling mode theory, there is no variable that represents the current to perform this phase changing characteristics. As a result, Γ_s should be complex instead of scalar in the model. However, it is a really complicated task to build a complex loss parameter for a MRC system. Therefore, it was simplified to scalar to simplify the analysis. Meanwhile, in the next section the problem can be solve by a circuit parameters based circuit model.

III. TRANSMISSION CHARACTERISTIC MODEL

In the former section, the energy distribution models of two kinds of topologies were presented. For the four-coil MRC system, the transmitting and receiving unit transmits energy by means of the inductive coupling and respective resonance coil. Therefore, it is necessary to introduce the inductive coupling link for building the transmission characteristics of the whole system.

A. Distance extension model of the chain topology.

The circuit equation of the single relay chain topology can be expressed as equation (16).

$$\begin{cases} \vec{I}_1 Z_1 + j\omega \vec{I}_2 M_{12} = \vec{V}_s \\ \vec{I}_2 Z_2 + j\omega(\vec{I}_1 M_{12} - \vec{I}_{rp} M_{2rp}) = 0 \\ \vec{I}_{rp} Z_{rp} + j\omega(\vec{I}_2 M_{2rp} - \vec{I}_3 M_{rp3}) = 0 \\ \vec{I}_3 Z_3 + j\omega(\vec{I}_{rp} M_{rp3} - \vec{I}_4 M_{34}) = 0 \\ \vec{I}_4 Z_4 + j\omega \vec{I}_3 M_{34} = 0 \end{cases} \tag{16}$$

Where, $\vec{I}_1, \vec{I}_2, \vec{I}_{rp}, \vec{I}_3, \vec{I}_4$ represent the current in the exciting

coil, sending coil, repeater coil, receiving coil and load coil. For computing convenience let:

$$M_{2rp} = M_{rp3}, \text{where } M_{rp3} = k_{rp3}\sqrt{L_{rp}L_3}$$

Solving the above equations, formula (17) can be obtained.

$$\eta = \mathrm{Re}\left(\vec{I}_4^{\,2} Z_4 \frac{1}{V_s^2} \Big/ \frac{\vec{I}_1}{V_s}\right) = \frac{\left(k_{12}k_{2rp}k_{rp3}k_{34}\sqrt{Q_1Q_2}\sqrt{Q_2Q_{rp}}\sqrt{Q_{rp}Q_3}\sqrt{Q_3Q_4}\right)^2}{\left[\begin{array}{l}-1-k_{12}^{\,2}Q_1Q_2+k_{2rp}^{\,2}Q_2Q_{rp}+k_{rp3}^{\,2}Q_{rp}Q_3+k_{34}^{\,2}Q_3Q_4\\+k_{12}^{\,2}k_{2rp}^{\,2}Q_1Q_2Q_{rp}Q_3+k_{12}^{\,2}k_{34}^{\,2}Q_1Q_2Q_3Q_4-k_{rp3}^{\,2}k_{34}^{\,2}Q_2Q_{rp}Q_3Q_4\end{array}\right]} * \frac{-1}{-k_{rp3}^{\,2}Q_{rp}Q_3+1-k_{34}^{\,2}Q_3Q_4-k_{rp3}^{\,2}Q_{rp}Q_3+k_{rp3}^{\,2}k_{34}^{\,2}Q_2Q_{rp}Q_3Q_4} \quad (17)$$

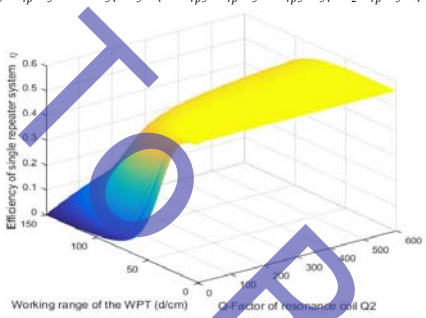

Fig.11 Transmission efficiency of a single relay system.

The transmission efficiency model is shown in Figure 11. When the Q value of the resonant coil of the relay system is higher than 500, the system can maintain more than 60% of the energy transfer efficiency under a transmission distance of 110cm. The repeater coil greatly increases the transmission distance. In order to analyze the effects of the air gap and Q on the transmission efficiency, figure 13 shows the detailed information in figure 12.

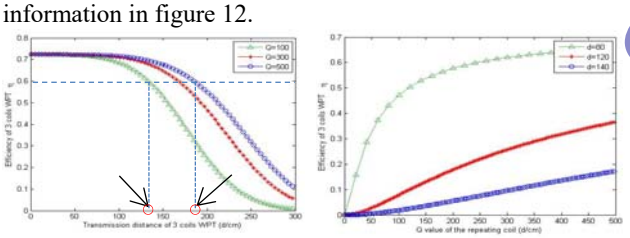

(A) Efficiency vs. distance. (B) Efficiency vs. Q value.

Fig.12 Transmission efficiency with specific values of *Q* and *d*.

In Fig. 12(A), three specific Q values and their corresponding transfer characteristic curves are drawn. Take 100 and 500 Q value as an example, air gap is extended to 185cm when the Q value is set to 500 whereas the air gap is 130cm when the Q value is set to 100. This comparison is done under the situation when the transmission efficiency η is 60% and the working frequency ω is more than 6MHz. Therefore, the higher the Q value is, the longer the available wireless energy can reach.

Figure 12 (B) shows the effect of the Q value on the transmission efficiency with different length of the air gap. The green line, red line and blue line represent 80cm, 100cm and 120cm of air gap, respectively. As for the 80cm case, the increasing of Q has an obvious effect on improving the transmission efficiency of the system whereas the 100cm and 120cm cases shows less transmission efficiency improving. This is mainly because at such distances, the system is working in the loose coupling state. Therefore, Q no longer plays a key role in transmission efficiency.

In addition, by way of constant parameter conformity, formula (17) can be transformed to formula (18).

$$\eta = \frac{C_1\left(k_{12}k_{23}\right)^2}{(C_2 + C_3k_{12}^{\,2} + k_{23}^{\,2}C_4)(C_5 + C_6k_{23}^{\,2})} \quad (18)$$

Where C_1, C_2, C_3, C_4, C_5 and C_6 are constants. It can be concluded that when the coupling coefficient k_{12} is equal to k_{23} under the condition that $k_{12}+k_{23} \leqslant M$ (where M is constant because the total distance between sending coil and receiving coil are preset, the value of $k_{12}+k_{23}$ has upper limit M, and M is given as 0.9), the energy received by the receiving coil reaches the maximum point. If only the sending coil and receiving coil are identical, the conclusion is established. In other words, if the sending coil and the receiving coil are not identical, the conclusion is incorrect in this model.

The repeater coil can greatly improve the transmission characteristics. If the repeater coil has good transmission characteristics, the transmission efficiency of the repeater system is not low although an extra impedance loss and radiation loss is introduced by the repeater coil. If the Q value of the repeater coil is high and the resonance frequency is turned precisely, a MRC system with a repeater coil can achieve a high transmission efficiency.

B. Energy allocation model of the branch topology

As for the branch topology, coupling exists between the three resonant coils. The circuit function can be expressed as function (19).

$$\begin{cases} \dot{I}_1Z_1 + j\omega\dot{I}_2M_{12} + j\omega\dot{I}_3M_{13} = V_s \\ \dot{I}_2Z_2 + j\omega\dot{I}_1M_{12} - j\omega\dot{I}_3M_{23} = 0 \\ \dot{I}_3Z_3 + j\omega\dot{I}_1M_{13} + j\omega\dot{I}_2M_{23} = 0 \end{cases} \quad (19)$$

The solution of the current for each coil is expressed by formula (20).

$$\begin{pmatrix} \dot{I}_1 \\ \dot{I}_2 \\ \dot{I}_3 \end{pmatrix} = \begin{pmatrix} \dfrac{(-Z_2Z_3 + \omega^2M_{23}^{\,2})V_s}{\omega^2M_{12}^{\,2}Z_3 + Z_1Z_2Z_3 - Z_1\omega^2M_{23}^{\,2} + \omega^2M_{13}^{\,2}Z_2} \\ \dfrac{j\omega V_s(M_{12}Z_3 + j\omega M_{23}M_{13})}{\omega^2M_{12}^{\,2}Z_3 + Z_1Z_2Z_3 - Z_1\omega^2M_{23}^{\,2} + \omega^2M_{13}^{\,2}Z_2} \\ \dfrac{\omega V_s(jM_{13}Z_2 + \omega M_{12}M_{23})}{\omega^2M_{12}^{\,2}Z_3 + Z_1Z_2Z_3 - Z_1\omega^2M_{23}^{\,2} + \omega^2M_{13}^{\,2}Z_2} \end{pmatrix} \quad (20)$$

1) Analysis of parameter S_{21}

The transmission function of the branch case is shown in formula (21).

$$\begin{cases} G_{21} = \dfrac{U_2}{U_1} = \dfrac{\dot{I}_2Z_2}{\dot{I}_1Z_1} \\ G_{31} = \dfrac{U_3}{U_1} = \dfrac{\dot{I}_3Z_3}{\dot{I}_1Z_1} \end{cases} \quad (21)$$

According formulas (20) and (21), the parameter S_{21} and S_{31} can be deduced, and they are shown in figure 13.

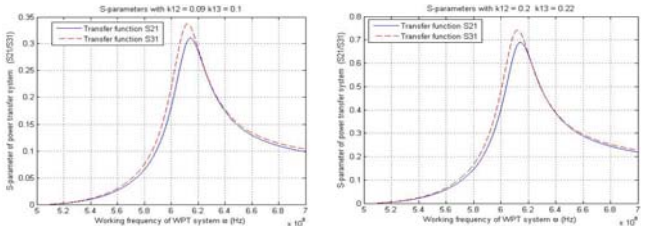

(A) S_{21} . (B) S_{31} .

Fig.13 the parameter S_{21} and S_{31} of a multi-loads system.

Parameter condition: figure (A): k_{12}=0.09, k_{13}=0.1; figure (B): k_{12}=0.2, k_{13}=0.22. In figure (A), the S_{21} , S_{31} parameters are distributed in the region of 0.3~0.35. In figure (B), the S_{21} , S_{31} parameters are distributed in the region of 0.65~0.75. The curves in the figure show the higher coupling coefficient companied with the higher *S* parameter. Therefore, in the two load branch case, the coupling coefficient still plays a key role in system's transmission characteristics. The working frequency at which S_{21} gets the maximum point is 6.15MHz. This is decided by the *C* and *L* parameters of the resonant coils used in the experiment.

2) Computing of the transmission efficiency η_{12} and η_{13} .

In branch applications, the most important thing is the working frequency's effect on the transmission efficiency and the distribution of the energy between different loads. The transmission efficiency model is expressed as formula (22).

$$\begin{cases} \eta_{21} = \dfrac{Re[W_2]}{Re[W_1]} = \dfrac{Re[\dot{I}_2^2 Z_2]}{Re[V_s \dot{I}_1]} \\ \eta_{31} = \dfrac{Re[W_3]}{Re[W_1]} = \dfrac{Re[\dot{I}_3^2 Z_3]}{Re[V_s \dot{I}_1]} \end{cases} \tag{22}$$

Where η_{21} and η_{31} represent the transmission efficiencies of *load2* and *load3*, respectively. The model is shown in figure 14.

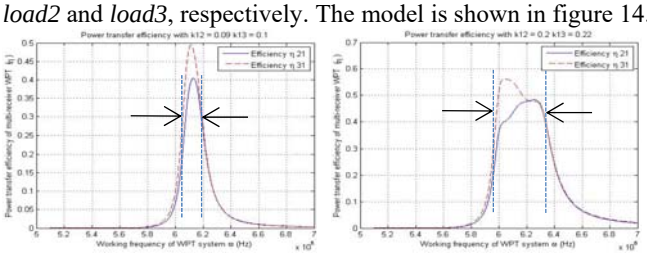

(A)k_{12}=0.09，k_{13}=0.1. (B)k_{12}=0.2，k_{13}=0.22.

Fig.14 Transmission efficiency of different loads with different coupling coefficients.

Since the two coupling coefficients are different, the transmission efficiencies are not equal. In figure (A), the maximum points of *load1* and *load2* are 45% and 50%, respectively. The system is working in the critical coupling state. Thus, the frequency width is relatively narrow. In figure (B), the maximum points of *load1* and *load2* are 48% and 57%, respectively. The system is working in the strong coupling state. Thus, the frequency width is wider than that of figure (A). In the strong coupling state, the system is not so critical or sensitive to its working frequency. However, this is at the cost of transmission distance.

C. Energy distribution model of the branch topology.

1) Distribution of the energy received by two loads.

The energy storage formula of the resonance coil is as shown in formula (23).

$$\begin{cases} W_2 = \dfrac{1}{2}\left|\dot{I}_2\right|^2 L_2 \\ W_3 = \dfrac{1}{2}\left|\dot{I}_3\right|^2 L_3 \end{cases} \tag{23}$$

The energy distribution model in between the two loads can be deduced from formula (20) and formula (23). Figure 15 shows the energy distribution of the multi-loads system under different coupling strengths.

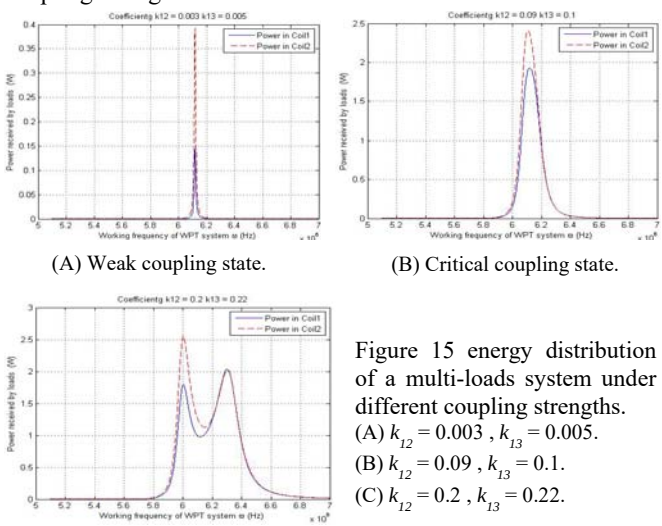

(A) Weak coupling state. (B) Critical coupling state.

(C) Strong coupling state.

Figure 15 energy distribution of a multi-loads system under different coupling strengths.
(A) k_{12} = 0.003 , k_{13} = 0.005.
(B) k_{12} = 0.09 , k_{13} = 0.1.
(C) k_{12} = 0.2 , k_{13} = 0.22.

As shown in figure 15, the following conclusions can be derived. Firstly, the energy transmission capacities of both routines are different under different coupling situations. The state of the strong coupling has a higher energy transmission capability than the weak coupling situation. The receiving powers are 0.4 and 2.4, as shown in figure (A) and figure (C). In addition, in the same working situation, a load with a higher coupling coefficient can receive more energy than a load with a lower coupling coefficient. The specific energy distribution principle is detailed in the following section. Furthermore, the frequency width under which the loads can receive power is different as shown in figure 16. Under the weak coupling situation, the frequency width is narrow. Meanwhile, the strong coupling state has the widest frequency range.

2) Coupling coefficient and energy distribution.

The principle for how the coupling coefficient affects the ratio of the energy distribution between loads is a key issue for the application of branch topology MRC systems. By an analysis of the coupling mode theory, formula (12) and formula (13) have been derived. According to formulas (19) and (22):

$$W_1 : W_2 = \frac{\left|jM_{12}Z_3 - \omega M_{23}M_{13}\right|^2}{\left|jM_{13}Z_2 + \omega M_{12}M_{23}\right|^2} = \frac{k_{12}^{\ 2}}{k_{13}^{\ 2}} \tag{24}$$

This is consistent with the CMT based analysis. Take k_{12} as a variable, when k_{12} varies from 0 to 0.2, experimental results of the circuit model are shown in figure 16.

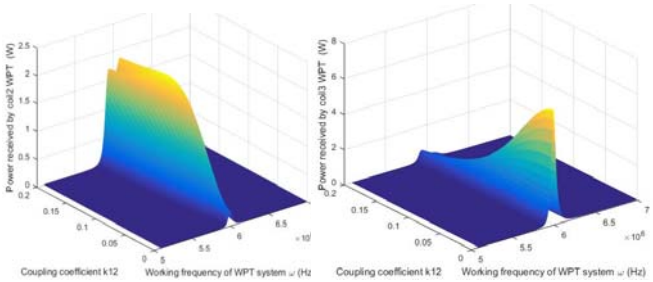

(A) Energy received by load1. (B) Energy received by load2.

Fig.16 Energy output distribution of a MRC system in a multi-loads application.

When k_{12} increases, the coupling strength between the source resonance coil and *load1* is enhanced. The two get into the strong coupling state when k_{12} is higher than the critical coupling point. Under the strong coupling situation, the amount of received power does not increase with k_{12} any longer, and it is almost kept stable. When *load1*'s coupling coefficient is increasing, the energy received by *load2* is decreasing by the inverse square law of the coupling coefficient k_{12}. Namely, when *load1*'s coupling is enhanced, more energy goes into *load1* which makes it seem as if *load1* has grabbed energy from *load2*. Therefore, if the physical characteristic of a MRC system is configured, the energy distribution between the loads obeys the model as shown in formulas (13) and (24).

IV. Experimental Verification

The experimental environments of the topology structures are built, and the transmission characteristics and energy resonance of the topology system are verified by experiments. The parameters of the sending resonant coil, receiving resonant coil and repeater resonant coil are provided in table I and table II.

Table I - Parameters of the Resonance Coils

Experimental parameters	Value (unit)
Input voltage V1	0.2(V)
Working frequency ω	6.2 (MHz)
Input impedance R_s	50(Ω)
Excitation coil impedance R_1, R_4	0.01(Ω)，0.01(Ω)
Resonant coil impedance R_2 R_3	0.1(Ω)，0.1(Ω)
Resonant coil inductor L_1, L_4	4.2(μH)，7.3(μH)
Resonant coil L_2, L_3	446(μH)，423(μH)
Excitation capacitor C_1 C_4	261(pF)，253(pF)
Resonant capacitor C_2 C_3	210.04(pF)，219.5(pF)
Resonant coil Q value Q_2,Q_3	545，572

Table II - Parameters of the Relay Coil

Coil parameters	Value (unit)
Working frequency ω	6.2 (MHz)
Resistance R_r	0.13(Ω)，0.1(Ω)
Inductance L_r	513(μH)
Resonant capacitor C_r	186 (pF)
Coil Q value Q_r	528

A. *Chain topology transmission experiment.*

The chain MRC wireless energy transfer experiment environment is shown in Figure 17. An 8W bulb was lit up at a distance of 160cm.

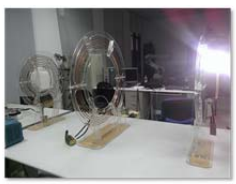

（A）Maximum transmission efficiency test $k_{12} = k_{13}$.

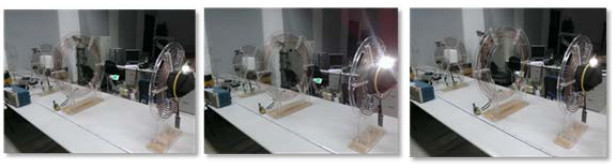

（A）d12=70cm,d23=90cm. （B）d12=80cm,d23=80cm. （C）d12=90cm,d23=70cm.

Fig.17 MRC-WPT experiment with one resonance repeater.

In the experiment, three pairs of k_{12}, k_{13} were tried to verify the effect of the coupling coefficient on the transmission characteristics. The distance test conditions between *S* and *R*, and between *R* and *D* are shown in Table III:

Table III - Relay Experiment

Distance relation	Coupling coefficient relation
d12=70cm,d23=90cm	$k_{12} > k_{23}$
d12=75cm,d23=85cm	$k_{12} > k_{23}$
d12=80cm,d23=80cm	$k_{12} = k_{23}$
d12=85cm,d23=75cm	$k_{12} < k_{23}$
d12=90cm,d23=70cm	$k_{12} < k_{23}$

Compared with the two resonant coils system, the transmission distance is significantly increased in the chain topology. The transmission distance is increased from 90cm to 160cm, and the effective transmission distance is increased by 77%.

A comparison of the transmission characteristics between the experimental results and the analytic solutions are shown in Figure 18. Although errors exist, the experiment results obeys the result of numerical simulation results. The experimental results of the S parameter are lower when compared to the theoretical results. Figure 18 (B) shows that the energy transfer efficiency is still higher than 50% in the chain setup without any optimization of the analog circuit or control method.

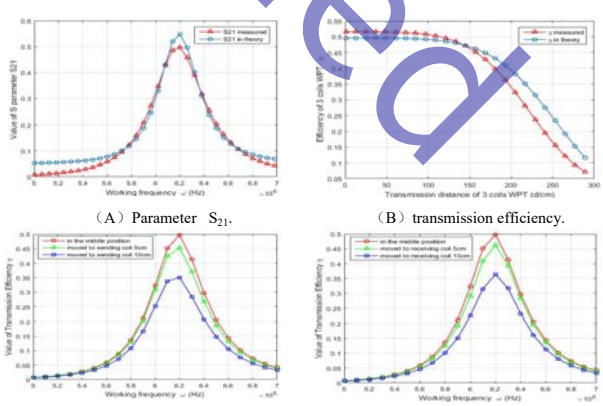

（A）Parameter S_{21}. （B）transmission efficiency.

（C）$k_{12} > k_{23}$. （D）$k_{12} < k_{23}$.

Fig.18 Experimental results of a distance deviation test for the chain topology.

Figure 18 (C) and (D) are the cases when the position of the repeater coil is tuned (5cm and 10cm towards the sending coil and the receiving coil, respectively). Therefore, when the repeater coil leaves the critical point (middle position), the transmission efficiency of the system is decreased. The longer the moving distance is, the less the transmission efficiency is reduced. When the coil is located in the middle position (k_{12}=k_{23}), the transmission efficiency reaches the maximum. Therefore, for a single repeater MRC system, the maximum transmission efficiency and transmission capacity can be obtained under the condition k_{12}=k_{23}. The power transfer efficiency of the system obviously decreases when the repeater coil is off the center position. For the two cases of k_{12}>k_{23} and k_{12}<k_{23}, the reduction of the energy transfer efficiency of the system is theoretically the same.

Diagrams of the received energy vs. k_{12} is shown in figure 19.

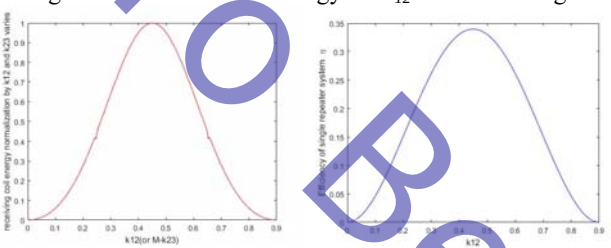

(A) Result under the coupling mode theory. (B) Result under the circuit analysis theory.

Fig.19 Received energy vs. k_{12} for the receiving coil in the chain topology.

When k_{12} = k_{23}, the energy received by the receiving coil reaches the maximum point. At this critical time, the resonance amplitude and voltage of the repeater coil reached their maximum states. Air ionization breakdown appears and is as shown in figure 20 when a small capacitor is used. By tuning k_1, k_2, if k_1=k_2, the repeater coil reaches the maximum resonance stage point. If a breakdown flash appears, replace it with a bigger capacity, and the breakdown phenomenon disappears.

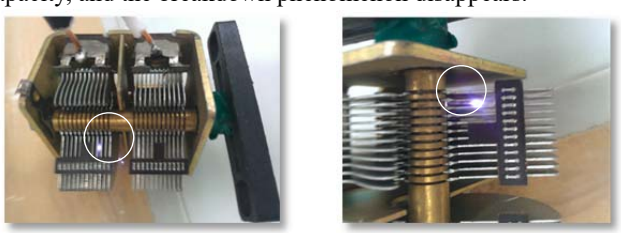

Fig.20 Breakdown phenomenon appears when the system reaches the critical point as k_1 = k_2.

B. *Branch topology transmission experiment.*

An experiment of the branch topology structure of MRC wireless energy transfer is shown in Figure 21. In the experiment, the 4 relative position relations of the branching topology are shown, and two 8W bulbs were lit up.

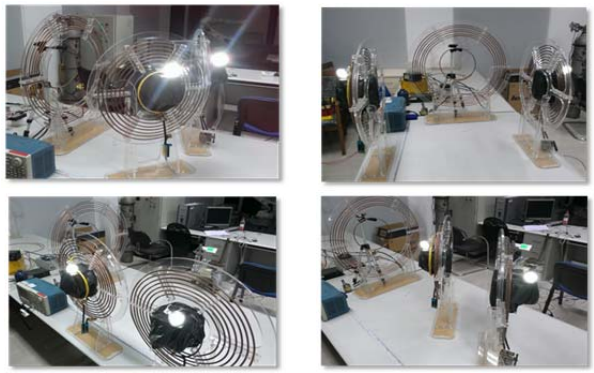

Fig.21 Branch topology experiment for a two loads case.

Experimental and theoretical analysis results are compared as shown in figure 22.

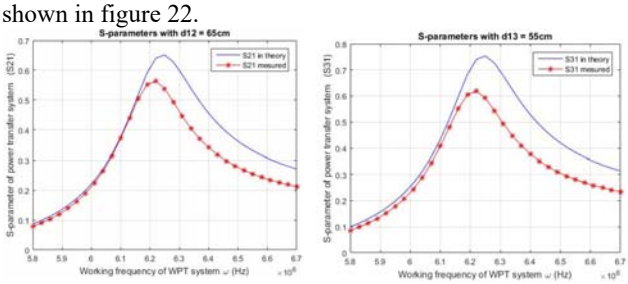

(A) S_{21} parameter of load1. (B) S_{31} parameter of load2.

Fig.22 Transmission characteristics of a two-load system.

Under the situation of k_{12}<k_{13}, the maximum value of the S_{21} parameter of *load1* is 0.57, the maximum value of the S_{31} parameter of *load2* is 0.62, the measured results of the energy transfer efficiency are 0.69 and 0.72, and the transmission efficiency of *load2* is higher than that of *load1*.

Figure 23 (A) and figure 23 (B) show the received power of *load1* and *load2* when k_{12} is increased. During this process, the energy received by *load1* is gradually increased, the energy received by *load* 2 is gradually reduced, and their sum is kept constant. This shows that the energy is moving from load2 to load1 when the coupling coefficient is tuned. The experimental results verify the correctness of the provided dynamic model for the "energy contention" between loads in the branch topology.

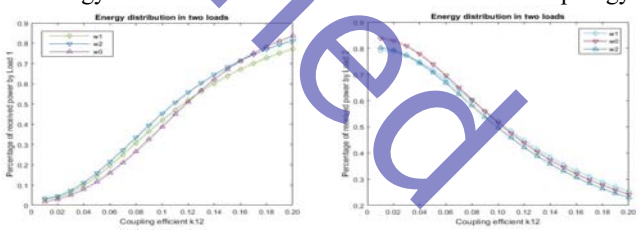

(A) Energy received by load1 when k_{12} varies. (B) Energy received by load2 when k_{12} varies.

Fig.23 Percentage of energy received by each of the two loads.

Deviation exists in both the chain topology experiment and in the branch topology experiment. The deviation between the experimental results and the theoretical results was caused by the deviation between the theoretical value and the actual value of elements' reactance, by the approximation of the k-d model (coupling coefficient - distance model), by the approximation of

the solution and by the assumption of the consistency of the resonant coils. The existence of these unavoidable situations leads to deviations. However, the correctness of the research is uninfluenced

V. Conclusion

In this paper, energy oscillation models for main topologies of MRC-WPT system were presented. These included the chain topology and the branch topology. In terms of the chain topology, the energy relaying model between the three coils in time domain are given. In terms of the branch topology, the energy distribution between the two loads are given. The energy relay model for the chain topology and energy distribution model for the branch model are deduced. Analysis are verified by actual experiments. In addition, the maximum resonance voltage was observed and the breakdown phenomenon was captured which verified that under the critical point of the working frequency, the voltage of the resonance reached the maximum point. A transmission model with an input term and loss item is established. The numerical simulation for the law of energy resonance is carried out for both topologies, and the correctness of the models is verified by experiments. The relay transmission efficiency is verified through three experiments with different coupling coefficients. The energy distribution and contention models are verified by branch topology experiments.

Acknowledgment

The authors gratefully acknowledge the Natural Science Foundation of Beijing of China (3164041) for its financial support.

References

[1] ThiQuynh VanHoang, Arnaud Breard, Christian Vollaire, "Near Magnetic Field Coupling Prediction Using Equivalent Spherical Hamonic Sources," in IEEE Transactions On Electromagnetic Compatibility. Vol. 56, No. 6, pp.1457-1465. December 2014.

[2] Kang Hyun Yi, "6.78MHz Capacitive Coupling Wireless Power Transfer System," in Journal of Power Electronics. Vol.15, no.4. pp.987-993, July, 2015.

[3] O. Jonah and S. V. Georgakopoulos, "Wireless Power Transfer in Concrete via Strongly Coupled Magnetic Resonance," in IEEE Transactions on Antennas and Propagation, vol. 61, no. 3, pp. 1378-1384, March 2013.

[4] W. Zhong and S. Y. R. Hui, "Auxiliary Circuits for Power Flow Control in Multifrequency Wireless Power Transfer Systems With Multiple Receivers," in IEEE Transactions on Power Electronics, vol. 30, no. 10, pp. 5902-5910, Oct. 2015.

[5] Xinzhi Shi, Chang Qi, Houxiang Xu and Shuangli Ye, "Study of wireless energy transfer by magnetic resonance coupling with two loads," in IECON 2016 - 42nd Annual Conference of the IEEE Industrial Electronics Society, pp. 4565-4569. December, 2016.

[6] J. P. K. Sampath, D. M. Vilathgamuwa and A. Alphones, "Efficiency Enhancement for Dynamic Wireless Power Transfer System With Segmented Transmitter Array," in IEEE Transactions on Transportation Electrification, vol. 2, no. 1, pp. 76-85, March 2016.

[7] S. H. Lee and R. D. Lorenz, "Development and Validation of Model for 95%-Efficiency 220-W Wireless Power Transfer Over a 30-cm Air Gap," in IEEE Transactions on Industry Applications, vol. 47, no. 6, pp. 2495-2504, Nov.-Dec. 2011.

[8] K. Sasaki, S. Sugiura and H. Iizuka, "Distance Adaptation Method for Magnetic Resonance Coupling Between Variable Capacitor-Loaded Parallel-Wire Coils," in IEEE Transactions on Microwave Theory and Techniques, vol. 62, no. 4, pp. 892-900, April 2014.

[9] J. M. Miller, O. C. Onar and M. Chinthavali, "Primary-Side Power Flow Control of Wireless Power Transfer for Electric Vehicle Charging," in IEEE Journal of Emerging and Selected Topics in Power Electronics, vol. 3, no. 1, pp. 147-162, March 2015.

[10] N. Y. Kim et al., "Automated adaptive frequency tracking system for efficient mid-range wireless power transfer via magnetic resonance coupling," in 2012 42nd European Microwave Conference, Amsterdam, pp. 221-224. 2012.

[11] H. Hwang, J. Moon, B. Lee, C. h. Jeong and S. w. Kim, "An analysis of magnetic resonance coupling effects on wireless power transfer by coil inductance and placement," in IEEE Transactions on Consumer Electronics, vol. 60, no. 2, pp. 203-209, May 2014.

[12] T. C. Beh, M. Kato, T. Imura, S. Oh and Y. Hori, "Automated Impedance Matching System for Robust Wireless Power Transfer via Magnetic Resonance Coupling," in IEEE Transactions on Industrial Electronics, vol. 60, no. 9, pp. 3689-3698, Sept. 2013.

[13] Y. Bu, M. Nishiyama, T. Ueda, Y. Tashima and T. Mizuno, "Examination of Wireless Power Transfer Combined With the Utilization of Distance Detection," in IEEE Transactions on Magnetics, vol. 50, no. 11, pp. 1-4, Nov. 2014.

[14] W. X. Zhong, C. K. Lee and S. Y. Hui, "Wireless power domino-resonator systems with noncoaxial axes and circular structures," in IEEE Transactions on Power Electronics, vol. 27, no. 11, pp. 4750-4762, Nov. 2012.

[15] H. D. Lang, A. Ludwig and C. D. Sarris, "Convex Optimization of Wireless Power Transfer Systems With Multiple Transmitters," in IEEE Transactions on Antennas and Propagation, vol. 62, no. 9, pp. 4623-4636, Sept. 2014.

[16] B. Luo, S. Wu and N. Zhou, "Flexible Design Method for Multi-Repeater Wireless Power Transfer System Based on Coupled Resonator Bandpass Filter Model," in IEEE Transactions on Circuits and Systems I: Regular Papers, vol. 61, no. 11, pp. 3288-3297, Nov. 2014.

[17] W. Zhong and S. Y. R. Hui, "Auxiliary Circuits for Power Flow Control in Multifrequency Wireless Power Transfer Systems With Multiple Receivers," in IEEE Transactions on Power Electronics, vol. 30, no. 10, pp. 5902-5910, Oct. 2015.

[18] Ping-an Tan, Haibing He, Xieping Gao, "A Frequency-Tracking Method Based on a SOGI-PLL for Wireless Power Transfer Systems to Assure Operation in the Resonant State," Journal of Power Electronics. Vol. 16, NO.3. pp.1056-1066. May 2016.

Mingbo Yang was born in China, in 1981. He received his B.S. degree in Electrical Control and Automation and his M.S. degree in

Navigation Guidance and Control from the Ordnance Engineering College, Shijiazhuang, China, in 2003 and 2008, respectively. He received his Ph.D. degree in Control Theory and Control Engineering from the Institute of Automation, Chinese Academy of Sciences, Beijing, China, in 2013. From 2013 to 2015, he was a Postdoctoral Fellow of Control Theory and Control Engineering in Tsinghua University, Beijing, China. Since 2015, he has been a Lecturer in the School of Mechanical and Materials Engineering, North China University of Technology, Beijing, China. His current research interests include wireless energy transmission, UPQC and embedded systems development.

Peng Wang was born in China, in 1981. He received his B.S. degree in Mechanical Engineering from the China University of Mining and Technology, Xuzhou, China, in 2004; and his Ph.D. degree in Mechanical Engineering from Beihang University, Beijing, China, in 2013. From 2013 to 2016, he was a Postdoctoral Fellow of Aeronautical and Astronautical Science and Technology at Beihang University. Since 2015, he has been a Visiting Scholar in the State Key Laboratory of Mechanical Transmissions, Chongqing University, Chongqing, China. Since 2016, he has been a Lecturer in the School of Mechanical and Materials Engineering, North China University of Technology, Beijing, China. His current research interests include gear geometry and soft robotics.

Yanzhi Guan was born in China, in 1981. He received his Ph.D. degree in Solid Mechanics from the Inner Mongolia University of Technology, Hohhot, China, in 2014. His current research interests include the development of mechatronics control systems and technology for variable cross-section roll forming.

Zhenfeng Yang was born in China, in 1987. He received his B.S. and M.S. degrees in Mechanical Design and Theory from the North China University of Technology, Beijing, China, in 2010 and 2013, respectively. His current research interests include the dynamics of mechanic electric systems and technology for variable cross-section roll forming.